Role of atomic charge transfer on sintering of TiO_2 nanoparticles: Variable-charge molecular dynamics

Shuji Ogata[a)]
Department of Applied Sciences, Yamaguchi University, Ube 755-8611, Japan

Hiroshi Iyetomi
Department of Physics, Niigata University, Niigata 950-2181, Japan

Kenji Tsuruta
Department of Electrical and Electronic Engineering, Okayama University, Okayama 700-8530, Japan

Fuyuki Shimojo
Faculty of Integrated Arts and Sciences, Hiroshima University, Higashi-Hiroshima 739-8521, Japan

Aiichiro Nakano, Rajiv K. Kalia, and Priya Vashishta
Concurrent Computing Laboratory for Materials Simulation, Louisiana State University, Baton Rouge, Louisiana 70803-4001

(Received 13 June 2000; accepted for publication 6 September 2000)

The stability of surface structure and space-charge distribution in free TiO_2 nanoparticles are investigated for both rutile and anatase phases using a variable-charge interaction potential in which atomic charges vary dynamically depending on their environment. We find the dynamic charge transfer: (i) enhances atomic diffusion at surfaces of the spherical nanoparticles at high temperatures; and (ii) creates additional repulsive force between the two nanospheres through formation of a double-charge surface layer in each nanosphere. The surface diffusion due to the charge transfer clearly distinguishes the two nanospheres with different underlying crystalline structures; the surface diffusion constant of the anatase sphere is almost three times as great as that of the rutile sphere. Variable-charge molecular dynamics simulations are then applied to sintering of two TiO_2 nanospheres. It turns out that the enhanced surface diffusion in the anatase nanosphere at high temperatures significantly promotes neck formation between the two spheres. © *2000 American Institute of Physics.* [S0021-8979(00)08323-7]

I. INTRODUCTION

Nanophase materials synthesized by consolidating nanometer-sized atomic clusters have attracted much attention in the last decade,[1] since nanophase materials often exhibit high strength,[1,2] high toughness,[1,2] and high catalytic reactivity[1,2] compared to conventional materials, due to the small size of individual phases. TiO_2 is one of the fundamental ceramics with a wide range of applications such as photocatalysts,[1–3] capacitors,[3] and pigments.[3] Those useful applications stem from its high electric permittivity[3] indicating large degrees of dynamic charge transfer between the atoms. The major phases of TiO_2 include the ground-state rutile[3] and the metastable anatase.[3] Despite their importance, little is known about the properties of TiO_2 nanoparticles and nanophase TiO_2.

TiO_2 nanoparticles may be synthesized by several methods.[1] In the gas-condensation method,[1,4,5] metallic Ti clusters coagulated on a cold surface are exposed to gaseous oxygen to form oxidized nanoparticles (TiO_{2-x}) with size[5] ~14 nm; their interior is rutile dominant.[5] In contrast, the sol–gel method[1,6,7] produces anatase nanoparticles of smaller sizes[6,7] (3–10 nm) with various degrees of aggregation[1,6,7] by precisely controlling the *p*H of the solution or doping surfactants. Those anatase nanoparticles sinter at lower temperatures[8,9] (~900 K) than the sintering temperature (~1300 K) of rutile nanoparticles.[5] During the sintering of anatase nanoparticles, an anatase-to-rutile phase transformation[8,9] has been found at the grain boundaries. Such low sintering temperatures are desirable for technical applications since grain growth is significantly suppressed during the sintering.[1] Theoretical investigation of sintering mechanisms of TiO_2 nanoparticles will offer valuable information for improved processing of nanoparticles.[1]

We have recently developed a variable-charge interatomic potential for molecular dynamics (MD) simulations of TiO_2 systems,[10] based on the pioneering work of Streitz and Mintmire.[11] In the potential, atomic charges vary dynamically depending on their environment to minimize the total potential energy.[10–12] The calculated pressure-dependent dielectric constants and surface energies of low-index planes for the rutile crystal as well as its cohesive energy, elastic moduli, and melting temperature, are in good agreement with experimental values.[10] The potential is also applicable to anatase; its experimental dielectric constants, cohesive energy, and lattice constants, are reproduced as well.[10]

In this article, we first analyze the stability of the surface structure and space-charge distribution in free anatase and rutile nanoparticles using the variable-charge interaction po-

a)Electronic mail: ogata@po.cc.yamaguchi-u.ac.jp

tential. We find that the dynamic charge transfer enhances atomic diffusion in surface regions of the spherical nanoparticles at high temperatures and also creates an additional repulsive force between the two nanospheres through formation of a double-charge surface layer in each nanosphere. The former effect should promote sintering of the nanospheres, whereas the latter may hinder sintering. To investigate their combined effects on sintering of TiO_2 nanoparticles, we then perform MD simulations of two nanospheres at various conditions using the established atomic potential. We show that the degree of diffusivity of surface atoms in nanospheres is a clue to explaining the different sintering behaviors between the rutile and the anatase nanoparticles.

This article is organized as follows. In Sec. II we analyze the properties of free anatase and rutile nanoparticles including their thermal stability. In Sec. III the space-charge distribution in the nanoparticles and its effects on interparticle interaction are analyzed. Section IV is devoted to the MD simulations of two nanoparticles at various conditions for both anatase and rutile phases to investigate the effects of the dynamic charge transfer on their sintering. Concluding remarks are given in Sec. V.

II. PROPERTIES OF FREE NANOPARTICLES

Anatase nanoparticles with size 70–100 Å processed in the sol–gel method[6,7] exhibit nearly spherical shapes. This observation indicates that the ground-state shape of an anatase nanoparticles in this range of diameter is a sphere. For comparison, we study the ground state of free rutile nanoparticles in the same size range by calculating the total potential energies of both spherical and faceted nanoparticles. We cut out rutile spheres with diameter $d=60$ and 80 Å from a rutile crystal, with the total number of atoms $N=10\,446$ and $N=24\,870$, respectively. The total potential energy $E_{\rm pot}$ of each nanosphere is minimized with respect to atomic positions and atomic charges using the conjugate gradient method. Faceted rutile nanoparticles with nearly the same numbers of atoms ($N=10\,164$ and $24\,102$) are also prepared following the Wulff construction[1] using the surface energies in Ref. 10. We find $E_{\rm pot}/N=-6.609$ eV for the nanosphere with $d=60$ Å ($N=10\,446$), $E_{\rm pot}/N=-6.601$ eV for the faceted nanoparticle with $N=10\,164$. The $E_{\rm pot}/N=-6.615$ eV for the nanosphere with $d=80$ Å ($N=24\,870$), $E_{\rm pot}/N=-6.608$ eV for the faceted nanoparticle with $N=24\,102$. Comparison of the energies indicates that the ground-state shape of a rutile nanoparticle with size 60–80 Å is spherical. In the following paragraphs we consider TiO_2 nanospheres with $d=60$ Å.

We investigate surface stability of the anatase and the rutile nanospheres by performing MD simulations with the variable-charge potential[10] for 18 ps at temperature $T=1400$ K. In the simulations we adopt the fast multipole method[13] for calculating Coulomb interactions efficiently, and the Nosé–Hoover thermostats chain[14] is used to control the temperature of the system. The MD time step is 0.37 fs. By calculating mean-square displacements of atoms $\langle|\Delta\mathbf{r}|^2\rangle$, we find that Ti and O atoms at radius $r>28$ Å are diffusing in both the anatase and the rutile nanospheres, while the interiors retain crystalline lattice structures. Diffusion constants[15] defined as $D_r=d\langle\Delta r_r^2\rangle/(2\Delta t)$ for the radial diffusion and $D_t=d\langle\Delta r_t^2\rangle/(4\Delta t)$ for the tangential diffusion with respect to Ti and O, are compared in Table I for the rutile and the anatase nanospheres. In the anatase nanosphere, $D_t=0.70(0.60)\times10^{-6}$ cm^2/s for Ti(O) is remarkably larger than $D_r=0.35(0.31)\times10^{-6}$ cm^2/s as well as $D_t=0.25(0.20)\times10^{-6}$ cm^2/s and $D_r=0.38(0.28)\times10^{-6}$ cm^2/s for Ti(O) in the rutile nanosphere. Such high tangential diffusion in the anatase nanosphere may be related to the experimental observation[16] that the anatase-to-rutile phase transformation begins at the surface of the bulk anatase if the temperature is kept at ~1000 K for hours. Slower diffusion of Ti and O that we find on the surface of the rutile nanosphere is expected since the melting temperature[8,10] of bulk rutile (~2200 K) is 1.6 times larger than the present temperature (1400 K).

TABLE I. Diffusion constants of Ti and O in the surface region ($r>28$ Å) of rutile and anatase nanospheres ($d=60$ Å) at $T=1400$ K. The D_r denotes the radial-diffusion constant; D_t, tangential-diffusion constant. Numbers in brackets are corresponding values in the rigid-ion cases.

	Anatase	
	$D_r(10^{-6}$ cm^2/s)	$D_t(10^{-6}$ cm^2/s)
Ti	0.35[0.18]	0.70[0.28]
O	0.31[0.15]	0.60[0.26]
	Rutile	
	$D_t(10^{-6}$ cm^2/s)	$D_t(10^{-6}$ cm^2/s)
Ti	0.38[0.27]	0.25[0.20]
O	0.28[0.21]	0.20[0.15]

To understand the effects of the charge transfer on atomic diffusion, we separately perform MD simulations for 18 ps in which the atomic charges are fixed to their bulk-crystalline values (i.e., rigid ion) at the ground state. For the anatase nanosphere we find $D_t=0.28(0.26)\times10^{-6}$ cm^2/s and $D_r=0.18(0.15)\times10^{-6}$ cm^2/s for Ti(O), as listed in brackets in Table I. For the rutile nanosphere, we find $D_t=0.20(0.15)\times10^{-6}$ cm^2/s and $D_r=0.27(0.21)\times10^{-6}$ cm^2/s for Ti(O). The charge transfer enhances both D_t and D_r by 90%–150% for the anatase nanospheres. Less enhancement in D_t and D_r, 20%–35%, is found for the rutile nanospheres. When the interatomic distance between a Ti and an O in the surface region is greater than the equilibrium value, charge transfer weakens their mutual binding by decreasing the magnitudes of the atomic charges, resulting in enhanced atomic diffusion. The difference in the enhancement factors of the diffusion constants between the rutile and the anatase nanospheres stems from their different internal structures.

III. SPACE-CHARGE DISTRIBUTION IN NANOPARTICLE AND INTERPARTICLE INTERACTION

Due to the charge transfer between atoms, the space-charge distribution is expected to be nonuniform in the nanospheres. Figure 1(a) shows the radial distribution of atomic

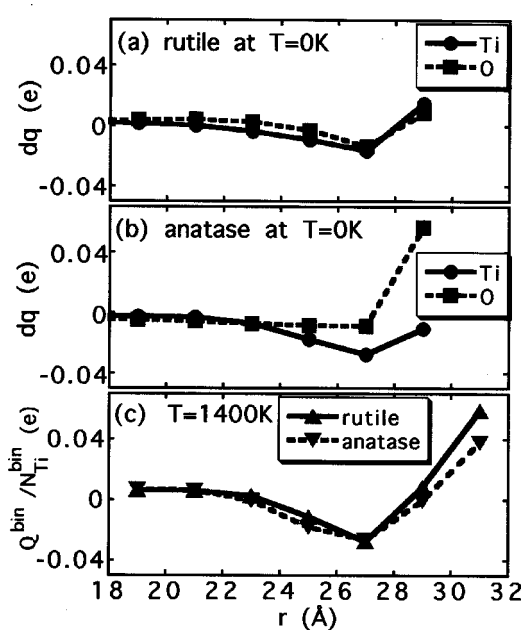

FIG. 1. (a) Value of dq for Ti and O in each radial shell for the rutile nanosphere ($d=60$ Å) at the ground state. (b) Same as (a) but for the anatase nanosphere. (c) Net charge normalized by the number of Ti atoms in each radial shell ($\Delta r=2$ Å) for rutile and anatase nanospheres at $T=1400$ K.

charges in the rutile nanosphere at the ground state, in which deviations of the charges from the bulk values, $dq=\langle q\rangle - q_{\mathrm{bulk}}$, with respect to Ti and O averaged in each radial shell ($\Delta r=2$ Å), are plotted. (The $q_{\mathrm{bulk}}=2.43e$ for Ti and $q_{\mathrm{bulk}}=-1.215e$ for O.[10]) Figure 1(b) shows the corresponding data for the anatase nanosphere at the ground state. Both for the rutile and the anatase nanospheres, the net charge of the surface region ($r=28-30$ Å) is positive while it is negative in the adjacent inner region ($r=24-28$ Å). This double-charge layer structure is maintained at an elevated temperature $T=1400$ K for both the rutile and the anatase nanospheres, as shown in Fig. 1(c). The Q^{bin} and $N_{\mathrm{Ti}}^{\mathrm{bin}}$ in Fig. 1(c) denote the net charge and the number of Ti atoms in each radial shell, respectively.

Angular distributions of the space charges in the rutile and the anatase nanospheres at 1400 K are shown in Fig. 2. In Fig. 2, atomic charges are averaged in voxels of size 3 Å×3 Å×3 Å, and the voxel charges in the region $z=[-3\text{ Å},3\text{ Å}]$ normalized by the number of Ti atoms are projected on the $x-y$ plane after averaging them for 18 ps. The horizontal axis in Fig. 2 corresponds to the ⟨100⟩ direction, the vertical axis to the ⟨010⟩. Distribution of the space charges is nearly spherical for both the rutile and the anatase nanospheres.

A similar double-charge-layer structure has been found for low-index surfaces of rutile in the calculations by Shelling, Yu, and Halley[17] for slab geometry using a tight-binding interaction potential. We calculate surface charges by taking two or three atomic layers in the slab, depending on the surface index, from the vacuum boundary so that the stoichiometry becomes Ti:O=1:2. We find that the surface charges per TiO_2 are $0.005e$ for the (110) surface, $0.01e$ for the (100), and $0.01e$ for the (001) in their tight-binding calculations. Despite differences in geometry, both the sphere and the slab systems form similar double-charge-layer structures.

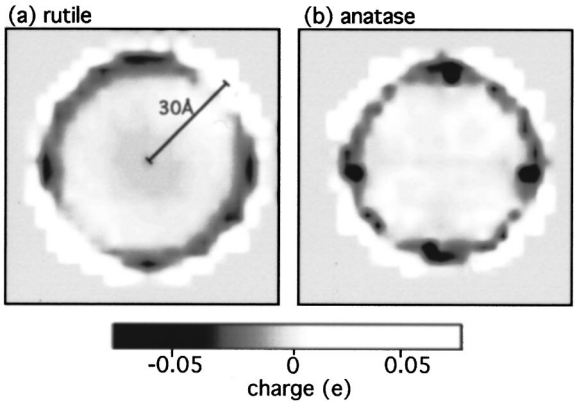

FIG. 2. (a) $x-y$ projection of space charges averaged over 18 ps in a slice $z=[-2\text{ Å},2\text{ Å}]$ of the rutile nanosphere ($d=60$ Å). (b) Same as (a) but for the anatase nanospheres.

Formation of the double-charge layer lowers the space-charge potential at the interiors. At $T=1400$ K, the net charge of the surface region ($r>28$ Å) is $Q\sim 17e$ for both the rutile and the anatase nanospheres. By modeling the double-charge-layer structure of a nanosphere as two parallel planes with surface charge densities $\pm 17e/[4\pi(28\text{ Å})^2]$ and distance 4 Å, we may estimate lowering of the potential at the interiors as $\Delta V=-1$ V. This value is greater in magnitude than the experimental values[18,19] $\Delta V=-0.1-0.2$ V for various kinds of grain boundaries in bulk rutile ($T=1650$ K).

The interaction potential between two nanospheres is affected by the double-charge-layer structure in each nanosphere. Let us denote the center-of-mass (COM) position of each nanosphere ($d=60$ Å) as $\mathbf{r}_{\mathrm{COM}}$. We evaluate the interparticle interaction-potential ΔE_{pot} of two nanospheres ($T=1400$ K) as a function of the distance between two COM's $R=|\Delta\mathbf{r}_{\mathrm{COM}}|$. Figure 3 shows ΔE_{pot} for three combinations of crystalline orientations. Both the ⟨100⟩ direction of one nanosphere and ⟨100⟩ of the other are parallel to the line connecting two COMs in the case ⟨100⟩-⟨100⟩; ⟨100⟩ and ⟨001⟩ in the case ⟨100⟩-⟨001⟩; and ⟨001⟩ and ⟨001⟩ in the case ⟨001⟩-⟨001⟩. The solid curves in Fig. 3 represent calculations that include dynamic charge transfer; while the dashed curves, the rigid-ion cases.

To obtain values plotted in Fig. 3 we first place two thermalized nanospheres at distance $R_0\equiv 69$ Å along the x axis. We then increase velocities of all the atoms in the smaller-x nanosphere by $\Delta v_x=100$ m/s, and similarly those in the larger-x nanosphere by $\Delta v_x=-100$ m/s. We perform the microcanonical MD simulation starting from that configuration. The value of ΔE_{pot} at $R(<R_0)$ we report is the negative of the change with respect to the total kinetic energies of the COMs. The same procedure is taken to evaluate ΔE_{pot} for two anatase nanospheres, and the results are shown in Fig. 4. For $R<62-62.5$ Å, Ti and O atoms on the contacting surfaces of the nanospheres slide to form a bridge between the two nanospheres in both the rutile and the ana-

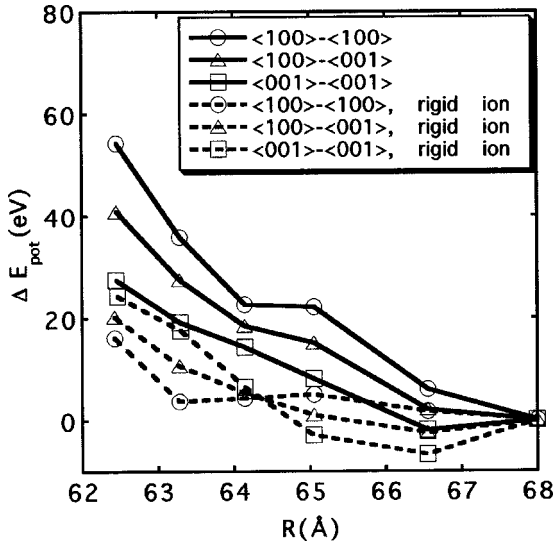

FIG. 3. Values of ΔE_{pot} as a function of R for two rutile nanospheres ($d=60$ Å) with various combinations of crystalline orientations. Solid curves correspond to the cases with variable-charge transfer included; dashed curves, to the cases in which atomic charges are fixed to their bulk-crystalline values at the ground state.

tase cases. The accuracy of ΔE_{pot} in Figs. 3 and 4 is estimated through comparison to the results with $\Delta v_x = \pm 150$ m/s: the possible uncertainty of ΔE_{pot} in Figs. 3 and 4 is 2–3 eV. We note that the dynamic charge transfer lowers the total potential energy of the two-nanosphere system at $R=69$ Å by $\sim 8.0\times 10^2$ eV for both the rutile and the anatase cases. For all R values, the total potential energy in the variable-charge case is substantially lower than that in the corresponding rigid-ion case. As seen in Figs. 3 and 4, increase in ΔE_{pot} becomes significant at $R<67$ Å for both the rutile and the anatase nanospheres.

In the variable-charge calculations (solid curves in Figs. 3 and 4), one may expect formation of macroscopic electric dipoles in the nanosphere, relating to large static dielectric constants[10] $\epsilon\sim 114$ for bulk rutile and ~ 46 for bulk anatase.

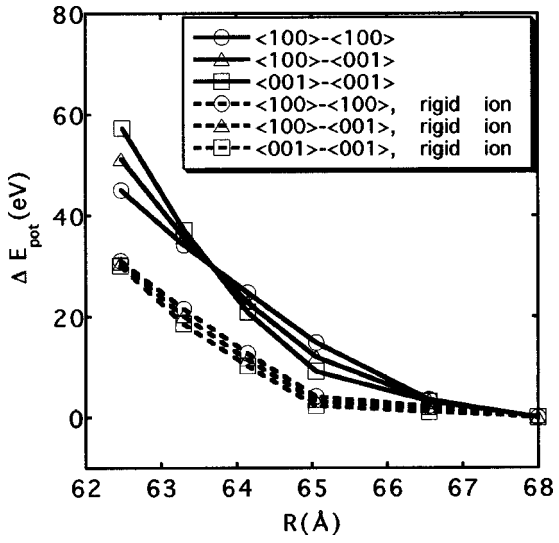

FIG. 4. Same as Fig. 3 but for the two anatase nanospheres.

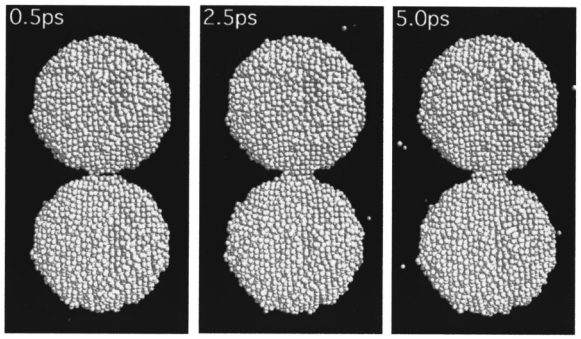

FIG. 5. Atomic configurations of two anatase nanospheres ($d=60$ Å) in the MD simulations at 1400 K with the ⟨100⟩-⟨100⟩ orientation. Only O atoms are shown by spheres.

Remembering that the short-range, non-Coulombic parts in the present interaction potential[10] have a cutoff distance at 9 Å, we investigate such a possibility by performing simulation runs of two nanospheres with their interparticle distance R fixed to ~ 69 Å. We, in fact, find in the runs that the macroscopic dipole–dipole interaction energies are within ± 0.1 eV, which are much smaller than values of ΔE_{pot} considered in Figs. 3 and 4.

We observe in Figs. 3 and 4 that the dynamic charge transfer adds repulsive interparticle force at $R=62-65$ Å for both the anatase and the rutile nanospheres. Since the surface region ($r>28$ Å) in each nanosphere has a net positive charge (Figs. 1 and 2), Coulomb repulsion between the two nanospheres results at close proximity. Comparing values of ΔE_{pot} at $R=62.5$ Å between the variable-charge and the rigid-ion cases, we find that the formation of the double-charge layer increases the contact potential by 10–30 eV for both the rutile and the anatase nanospheres.

IV. CHARGE TRANSFER AND SINTERING OF NANOPARTICLES

We perform variable-charge MD simulations to investigate the evolution of two nanospheres when they approach each other closer than $R\sim 61$ Å. Initial configurations for those simulation are prepared in four steps: (i) We take an atomic configuration with $R\sim 60$ Å in the MD run for evaluation of ΔE_{pot} in Figs. 3 and 4. (ii) The COM velocity of each nanosphere is set to zero by shifting velocities of all the atoms by the same amount. (iii) MD simulation is performed

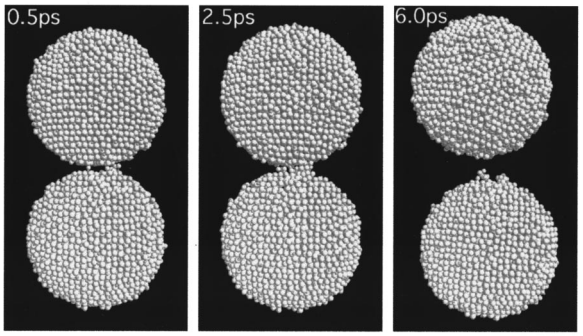

FIG. 6. Same as Fig. 5 but for two rutile nanospheres.

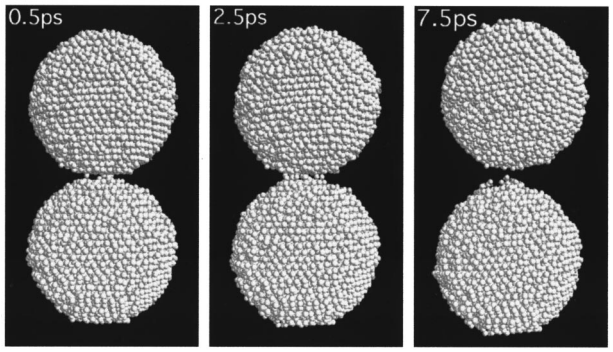

FIG. 7. Same as Fig. 5 but in the rigid-ion cases.

for 0.5 ps at $T=1400\,\mathrm{K}$. The interparticle separation becomes $R\sim 61\,\text{Å}$. (iv) The COM velocity of each nanosphere is reset to zero. We consider the same combinations of crystalline orientations as in the evaluation of ΔE_{pot} (Figs. 3 and 4): the $\langle 100\rangle$-$\langle 100\rangle$, the $\langle 100\rangle$-$\langle 001\rangle$, and the $\langle 001\rangle$-$\langle 001\rangle$, for both the rutile and the anatase nanospheres.

In the case of anatase nanospheres we find the onset of sintering after $\sim$ 5 ps irrespective of the lattice orientations. This is accompanied by surface atomic diffusion to form a neck between the two nanospheres, as depicted in Fig. 5. In the case of rutile nanospheres, on the other hand, R increases monotonically until they separate completely, as demonstrated in Fig. 6. The observed difference in sintering behaviors between the anatase and the rutile cases should originate from the difference in the diffusion constants of the surface atoms. Such high rates in sintering of the anatase nanospheres near the melting temperature are in accordance with the experimental results.[8,9]

In Secs. II and III, it has been found that dynamic charge transfer enhances atomic diffusion in surface regions of the nanoparticles at $T=1400\,\mathrm{K}$, whereas it creates additional repulsive interparticle force through formation of a double-charge surface layer in each nanoparticle. The first effect, which promotes sintering of nanoparticles, is more significant for the anatase than the rutile. The second effect, which may act to hinder sintering, is substantial for both the anatase and the rutile. To understand their combined effects, we separately perform rigid-ion MD simulations of two nanospheres for both the anatase and rutile phases. Both in the anatase and the rutile cases, the two nanospheres separate in $\sim$ 5 ps. Figure 7 depicts snapshots at 0.5, 2.5, and 7.5 ps in the rigid-ion MD run for the anatase nanospheres with the $\langle 100\rangle$-$\langle 100\rangle$ orientation. In the run, the two anatase nanospheres show no tendency to sinter during 10 ps and no substantial deformation is found in the surface regions. Accumulating the results, we conclude that the enhanced surface diffusion due to the charge transfer plays an essential role in the sintering of nanoparticles at high temperatures.

V. SUMMARY AND CONCLUDING REMARKS

We have investigated the stability of surface structure and space-charge distribution in free anatase and rutile nanospheres using a variable-charge interaction potential. We have found that the dynamic charge transfer enhances atomic diffusion in surface regions of the nanoparticles at $T=1400\,\mathrm{K}$ and that it creates additional repulsive force between the two nanoparticles through formation of a double-charge layer in each surface of a nanoparticle. We have performed variable-charge MD simulations to investigate their combined effects on sintering of two nanospheres and possible dependence of sintering mechanisms on the internal structures. We have found that sintering of two anatase nanoparticles is promoted significantly by the enhanced surface diffusion due to dynamic charge transfer.

The present MD results and analyses provide a basis for the future understanding of phase-transformation-assisted sintering of anatase nanoparticles,[8,9] which is a promising technique to produce high-quality nanophase TiO_2. Larger-scale, variable-charge MD simulations for sintering of nanoparticle-assembled TiO_2 are in progress.

ACKNOWLEDGMENTS

This work was performed under the Japan–U.S. Joint Research Program with support from JSPS and NSF. The authors would also like to acknowledge the support of U.S. DOE, AFOSR, ARO, USC–LSU Multidisciplinary University Research Initiative, NSF, and NASA.

[1] *Nanomaterials Synthesis, Properties, and Application*, edited by A. S. Edelstein and R. C. Cammarata (IOP, London, 1996).
[2] Y.-M. Chiang, D. Birnie III, and W. D. Kingery, *Physical Ceramics* (Wiley, New York, 1997).
[3] *Concise Encyclopedia of Advanced Ceramic Materials*, edited by R. J. Brook (Pergamon, Cambridge, 1991), pp. 486–488.
[4] R. W. Siegel, S. Ramasamy, H. Hahn, L. Zongquan, L. Ting, and R. Gronsky, J. Mater. Res. **3**, 1367 (1988).
[5] H. Hahn, J. Logas, and R. S. Averback, J. Mater. Res. **5**, 609 (1990).
[6] Q. Xu and M. A. Anderson, Mater. Res. Soc. Symp. Proc. **132**, 41 (1989).
[7] T. J. Trentler, T. E. Denler, J. F. Bertone, A. Agrawal, and V. L. Colvin, J. Am. Chem. Soc. **121**, 1613 (1999).
[8] K.-N. P. Kumar, K. Keizer, A. J. Burggraaf, T. Okubo, H. Nagamoto, and S. Morooka, Nature (London) **358**, 48 (1992).
[9] W. Ma, Z. Lu, and M. Zhang, Appl. Phys. A: Mater. Sci. Process. **66A**, 621 (1998).
[10] S. Ogata, H. Iyetomi, K. Tsuruta, F. Shimojo, R. K. Kalia, A. Nakano, and P. Vashishta, J. Appl. Phys. **86**, 3036 (1999).
[11] F. H. Streitz and J. W. Mintmire, J. Adhes. Sci. Technol. **8**, 853 (1994).
[12] F. H. Streitz and J. W. Mintmire, Phys. Rev. B **50**, 11996 (1994).
[13] L. Greengard and V. Rokhlin, J. Comput. Phys. **73**, 325 (1987).
[14] G. J. Martyna, M. E. Tuckerman, D. J. Tobias, and M. L. Klein, Mol. Phys. **87**, 1117 (1996).
[15] See, e.g., M. P. Allen and D. J. Tildesley, *Computer Simularion of Liquids* (Oxford Science, Oxford, 1989).
[16] R. D. Shannon and J. A. Pask, J. Am. Ceram. Soc. **48**, 391 (1965).
[17] P. K. Schelling, N. Yu, and J. W. Halley, Phys. Rev. B **58**, 1279 (1998).
[18] J. A. S. Ikeda and Y.-M. Chiang, J. Am. Ceram. Soc. **76**, 2437 (1993).
[19] J. A. S. Ikeda, Y.-M. Chiang, A. J. Garratt-Reed, and J. B. Vander Sande, J. Am. Ceram. Soc. **76**, 2447 (1993).